Sensors & Actuators: A. Physical 396 (2025) 117178

Contents lists available at ScienceDirect

Sensors and Actuators: A. Physical

journal homepage: www.journals.elsevier.com/sensors-and-actuators-a-physical

Air-coupled ultrasound transduction improvement using vertical piezoelements' array

Linas Svilainis [a,*], Valdas Eidukynas [b], Luca De Marchi [c], Andrius Chaziachmetovas [a]

[a] Department of Electronics Engineering, Kaunas University of Technology, Kaunas, Lithuania
[b] Department of Mechanical Engineering, Kaunas University of Technology, Kaunas, Lithuania
[c] Department of Electrical, Electronic, and Information Engineering "Guglielmo Marconi", University of Bologna, Bologna, Italy

ARTICLE INFO

Keywords:
Ultrasonic transducer
Air-coupled ultrasound
Transduction efficiency
Acoustic impedance matching

ABSTRACT

Novel transducer construction is proposed: array of PVDF film strips placed parallel to each other with air gaps between. Films are oriented in such way that strip extension (31 mode) is aligned with emission direction. Transduction is improved by providing better acoustic impedance match to air and increased displacement of emitting surface. Two distinct operation modes are presented: i) emission from the gaps ii) emission from membrane attached to the edges at array top with lower edges backed.

In gap emission mode, the transduction efficiency is increased because of two mechanisms. The pressure produced by the expansion of the individual films is concentrated into narrow gap. Also, emission of edges due to height extension. Height extension (31 mode) is much higher than thickness expansion (33 mode) if film height is larger than film thickness. Low, 500 Rayl, equivalent acoustic impedance of gap emission is achieved at film thickness 10 µm and gap with 50 µm.

In membrane emission mode, only extension (31 mode) is used, pressure emitted is increased due to large membrane displacement and better match to air. Equivalent acoustic impedance is 500 kRayl at PVDF film thickness 40 µm and 200 µm air gap. Displacement is maximized if PVDF film with large transverse piezoelectric coefficient d_{31} is used.

Experimental measurements are presented. Transmission sensitivity peak for gap emission was 155 mPa/V, for membrane emission mode it was 320 mPa/V. Impressive, more than 270 % fractional bandwidth was confirmed experimentally.

1. Introduction

Ultrasound offers a non-ionizing, noninvasive measurement and imaging technique for medicine and science. Piezoelectric phenomenon is most widely used for ultrasonic transducers [1–3]. Yet, coupling the piezoelement output to the propagation media is a major problem due to significant impedance mismatch. Therefore, ultrasonic measurements are usually is carried out in contact or immersion mode.

Air-coupled ultrasound is a non-contact measurement. Its value was already demonstrated for non-destructive testing [4–6], material properties measurement [7], imaging [8], production line control [9], gas flow sensing [10], food products [11] or plant studies [12]. However, the implementation of the air-coupled ultrasound is faced with the essential challenge: an impedance mismatch [13,14]. The acoustic impedance of air is low, about 413 Rayl. The acoustic impedance of piezoelectric materials is high: piezoelectric ceramics have 20–40 MRayl, single crystal: 15–20 MRayl, polymers 1–5 MRayl impedance. The impedance mismatch is 10 000–100 000 times. This mismatch locks the energy inside the piezoelement. Resonance occurs if delay of the ultrasonic wave propagation within the thickness of the piezoelement is comparable to the period of the frequency used. Transmission becomes narrowband, only frequencies around the thickness resonance (usually half of the wavelength in the piezoelement) are emitted. Then, essential advantage of the piezomaterials, ability to produce a large strain, is lost.

While small displacement is enough to produce a significant strain in solid material, transmission into air requires larger displacement. Otherwise, the intensity of the transmitted wave is low. The most common approach is to use a mechanical transformer. Most popular approach is a quarter wavelength matching layers [15,16], which not only increases the signal amplitude but also broadens the transmission

* Corresponding author.
E-mail address: linas.svilainis@ktu.lt (L. Svilainis).

https://doi.org/10.1016/j.sna.2025.117178
Received 9 July 2025; Received in revised form 29 August 2025; Accepted 15 October 2025
Available online 17 October 2025
0924-4247/© 2025 The Author(s). Published by Elsevier B.V. This is an open access article under the CC BY-NC-ND license (http://creativecommons.org/licenses/by-nc-nd/4.0/).

bandwidth. Yet, materials for outer layers demand properties that are at the edge of modern physics [17–19]. Despite impressive results (-20 dB bandwidth 80 %, transmission sensitivity 5–12 Pa/V, [24]) have been reported with specially selected and designed layers [15,17], design and assembly of such transducers requires extensive knowledge, skills and specific equipment. Metamaterial structures have been proposed for impedance matching [20–23]. Porous rubber metamaterials reported in [22] have reached 26 kRayl impedance (close to 7 kRayl required for 3 layer matching [16,17]). Yet, wavelength is very small due to low velocity (38.5 m/s), quarter wavelength layer thickness is 19 µm. Also, attenuation is high and frequency-dependent. These parameters render them suitable only for very low frequencies. Gradient impedance can be obtained if conical material structures are mixed [23], but such approach is only suitable for solid-solid materials matching and is able to cover relatively small (up to one order) impedance mismatch. Tapered cones, covered by thin membrane [20,21] act as impedance transformer and their suitability for water have been demonstrated, but again, geometry required for air is not physically realizable. Therefore, it is only suitable water (one order) impedance matching.

Broadband response can be achieved if piezoelement is operated below its resonance. Thin, 70 µm PVDF film use has been reported for reception [25,26,30], broad bandwidth was attained, but sensitivity was mere 0.2–0.4 µV/Pa, same should be applicable for transmission. Sensitivity loss can be compensated by higher excitation voltage. Unfortunately, high strain is produced in film, metallization quickly degrades at higher than 500 V voltage excitation.

Higher output pressure can be obtained by focusing [27,28], (e.g. focusing 20 mm diameter PVDF film into 1 mm spot would increase pressure 400 times), but focal spot size depends on frequency so less pressure will be produced for low frequencies, AC response will not be flat.

It is also possible to stack the PVDF films by placing several layers on top of each other [29,30] in order to increase the displacement and the resulting acoustic signal intensity. Yet, such approach has some limit for total thickness: operation will become resonant as soon as the stack thickness reach the half wavelength.

The approach proposed here is to use an array of PVDF films placed parallel to each other, but with air gaps between. Several operation modes can be used: i) emission from the gaps ii) emission from membrane attached to the edges at one end, iii) both ends or iv) lower edges backed. Emitted pressure is increased compared to conventional single-layer film case if gap emission is used, because pressure emitted by individual film is concentrated into narrow gap. PVDF film is also experiencing extension in transverse direction, this phenomenon is used if membrane emission is used. Detailed explanation is presented in next section.

2. Transducer design principles

Two proposed emission modes are explained in Fig. 1.

In both modes PVDF film is placed so that longitudinal expansion is in horizontal direction (refer Fig. 1). Longitudinal piezoelectric coefficient d_{33} (piezoelectric charge or displacement coefficient) quantifies the longitudinal strain (expansion of the film relatively to its thickness) under applied electrical field [31]. For PVDF it usually ranges from 20 to 34 pm/V (or pC/N for direct piezoelectric effect). This mode is usually used for hydrophones production. Since both strain and electrical field are normalized by same thickness, as long as operation is below the resonance frequency, absolute expansion amount does not depend on film thickness.

Under harmonic excitation, displacement magnitude Δt, caused by expansion, can be converted to the magnitude of the acoustic pressure produced in air Δp as:

$$\Delta p_{film} = Z_{air}\omega\Delta t, \tag{1}$$

where Z_{air} is air impedance, ω is the sinusoid angular frequency. In such case, if magnitude of excitation voltage is constant over frequency range, acoustic pressure, delivered to air will increase with frequency. Yet, with displacement produced in picometers and low (Z_{air}=413 Rayl) acoustic impedance, pressure produced is very low. Vertical placement of films is aimed to increase the pressure produced by gap emission, the resulting pressure from the gap cavity can be increased:

$$\Delta p_{cavity} = h\Big/(w+t)\Delta p_{film}, \tag{2}$$

If pitch of the film placement (w+t) is significantly smaller than the height h of the film array, pressure emitted from the cavity will increase. For instance, gain is 1000 with h= 10 mm and t = 4 µm, w= 6 µm.

Gap also acts as resonant cavity: if gap width is smaller than wavelength in air, resonance frequency is:

$$f_r = c_{air}/(2h), \tag{3}$$

where c_{air} is speed of sound in air. The gap width defines the quality: the smaller the w, the higher is the quality. With small (343 m/s) speed of sound in mind, it can be concluded, that array height is limited by λ/2. For 40 kHz h is limited to 4.3 mm and h is 0.35 mm at 500 kHz, but there are other phenomena, discussed further, that allow operation even beyond the resonance.

In energy harvesting, actuator applications it is usual for PVDF film to be operated in flextensional mode [31] because it has large transverse piezoelectric coefficient d_{31} which can be comparable or even higher than d_{33}. Therefore, with electrical field applied along direction 3 (horizontal in Fig. 1) there will be not just film expansion along direction

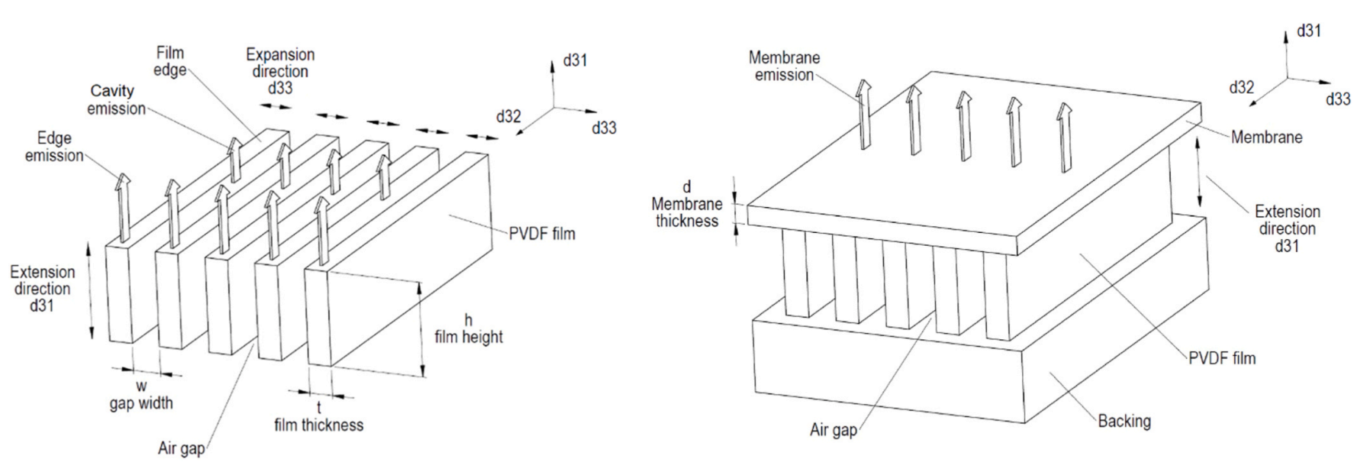

Fig. 1. Construction and PVDF film arrangement for (left) gap emission or (right) membrane emission.

3, but also extension along direction 1 (vertical in Fig. 1). The absolute extension Δh is defined by h/t ratio [42]:

$$\Delta h \sim d_{31}h \quad E = d_{31}h\Delta u/t, \tag{4}$$

where E is the electrical field strength (Δu/t), Δu is the excitation voltage. Compare to absolute expansion of PVDF film Δt [42]:

$$\Delta t \sim d_{33}t \quad E = d_{33}t\Delta u/t = d_{33}\Delta u, \tag{5}$$

Assuming comparable d_{33} and d_{31}, the absolute extension Δh when h $>>$ t will be significantly higher that Δt. Then, there is another source of emission, edge emission (refer Fig. 1 left). The AC response of emission will be defined by constructive or destructive interference of those two emission sources.

If film edges are covered by thin membrane, the edge emission will prevail. Several configurations are possible: one end or both can be covered by membrane, lower end can be backed and membrane placed on top. Fig. 1 right presents the latter case. In such case array of films acts as piezoelectric plate with new equivalent piezoelectric coefficient defined by Eq.(4) and lower acoustic impedance. According to [32], a membrane, loaded by fluid on one side and supported by an array of bars on another side transfers the bar acoustic impedance by bar width (in our case it is a film thickness) to pitch ratio. In other words, equivalent impedance Z_{eq} seen by fluid is defined by equivalent material density ρ_{eq} behind the membrane:

$$Z_{eq} = \rho_{PVDF} \bullet \frac{t}{w+t} \bullet c_{PVDF} = \rho_{eq} \bullet c_{PVDF}, VF = \frac{t}{w+t}, \tag{6}$$

where c_{PVDF} is speed of sound in PVDF film, ρ_{PVDF} is PVDF film density, Z_{PVDF} is film impedance and VF is volume fraction of PVDF film. In such case acoustic impedance is close to air. E.g., if c_{PVDF}= 1280 m/s and ρ_{PVDF} = 1780 kg/m^3 then Z_{PVDF} is 2.3 MRayl, much higher than Z_{air} (413 Rayl), but if t = 4 µm, w= 400 µm Z_{eq} seen by fluid is 100 times lower. Additionally, the equivalent stiffness (so the equivalent velocity) of the vertical film structure is also decreasing with VF reduction. Therefore, better impedance match to air is achieved and acoustic pressure delivered is higher.

It should be noted that PVDF film length is not considered: i) d_{32} is negligible compared to d_{33} and d_{31} ii) length will only affect the far-field performance, otherwise no effect in the near field, where measurements were carried out.

3. Performance evaluation by simulation

Performance evaluation and selection of optimal parameters of transducer made of such gapped array of PVDF films was carried out using finite element method (FEM) in COMSOL. Single PVDF film and gap around was simulated with periodic condition on both sides in 2D model (plane strain). Such approach simulates infinite transduction structure, facilitating simulation speed and avoiding transducer edge effects on transmitted field. Excitation waveform was a Gabor function with 150 kHz (for low frequencies performance evaluation) or 0.75 MHz (wideband studies) center frequency and 100 % bandwidth. Adaptive time step was used in simulation. Sampling frequency for measurement results extraction was 30 MHz, 40 times the sampling frequency. Quartic (fourth order) elements of maximum 80 µm were used. Simulation was carried out in time domain. Discrete Fourier transform (DFT) was used to transform the waveform into frequency domain.

3.1. Gap emission simulation analysis

Model geometry drawing, used for gap emission simulation, is presented in Fig. 2.

Built-in PVDF film material model was used with equivalent d_{33}= 33.8pC/N or pm/V d_{31}= 13.6pC/N and d_{32}= 1.5pC/N, equivalent compression wave velocity c_{PVDF}= 1280 m/s and ρ_{PVDF} = 1780 kg/m^3.

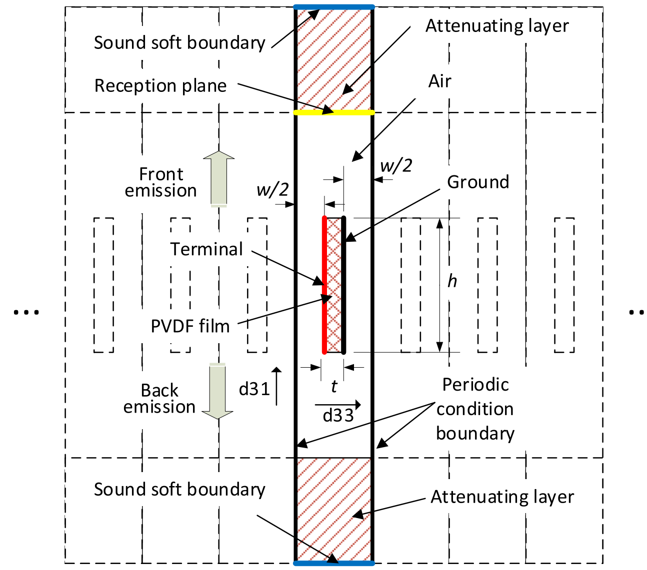

Fig. 2. FEM model used for gap emission simulation.

Film polarization was oriented is such way that the expansion (thickness) direction was aligned with d_{33} and the extension (height) direction was aligned with d_{31} (refer Fig. 2). Reception plane, that was used for transmitted pressure measurement, was placed at 1 mm distance from film edge. Pressure, registered at this plane was averaged along direction x to produce a single waveform. Attenuation layers were placed at top and bottom, spaced 1 mm from the film edge. Additionally, sound soft boundaries were placed at 2 mm from film edge in order to attain infinite space measurements. Air gap was placed at both sides of the film. Periodic condition boundary was placed at $w/2$ distance from the film to emulate the infinite array.

First, film height has to be established. Frequency range of interest was set to 50 kHz to 1 MHz. The lowest frequency is defined by reasonable near field distance: at 50 kHz and transducer diameter 20 mm near field distance is around 15 mm. Such distance corresponds to 44 µs delay in air, still suitable to avoid multiple reflections. The upper frequency range is limited by attenuation: frequencies beyond 1 MHz are more subjected to attenuation in air-coupled ultrasound. Simulation results presented in Fig. 3 demonstrate how emission is changing when h is 0.567 mm (corresponds to λ/2 at 300 kHz in air), 1.133 mm (λ/2 at 150 kHz), 1.7 mm (λ/2 at 100 kHz) and 2.266 mm (λ/2 at 75 kHz).

It can be noted that position of the fist peak (red curve) is as expected, e.g. 150 kHz at 1.2 mm. From Eq.(2) it can be expected that larger h will produce higher pressure. Pressure at resonant peak should be analyzed. Yet, pressure at h= 2.266 mm, 75 kHz is only slightly higher than at h= 0.567 mm, 300 kHz, but h has changed 4 times, should be + 12 dB. The reason is in Eq.(1): same displacement produces less pressure at lower frequencies.

Broader frequency range response at different t and w is presented in Fig. 4. Different values for t and w were used in order to make the pressure gain more pronounced.

First peak appears for array height h corresponding to λ/2 in air. For 750 kHz h should be ~230 µm. Then essential advantage is lost: h becomes comparable to PVDF film thickness t (commercially available range is 10–200 µm). Therefore, in next experiments, it was decided to use 150 kHz-matched or λ/2 h, roughly 1.2 mm. Such array height is optimal from the point of expected pressure gain, Eq.(2), from the technological point (smaller h is not easy to handle, especially in manual assembly) and is producing less resonance dips than at larger h values.

It can be noted that next peak does not correspond to thickness resonance. E.g., for 1.2 mm peaks should occur at 450 kHz, 750 kHz etc.

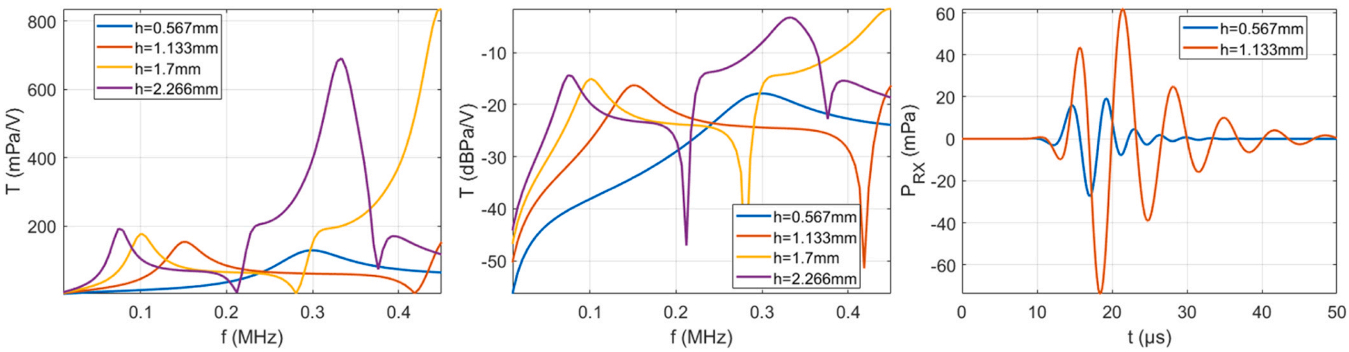

Fig. 3. Gap emission simulation when array height h is varied at fixed $t = 70$ μm $w = 20$ μm. Left: frequency domain sensitivity linear scale, center: logarithmic scale sensitivity, right: time domain response to 150 kHz, 100 % bandwidth Gabor function excitation.

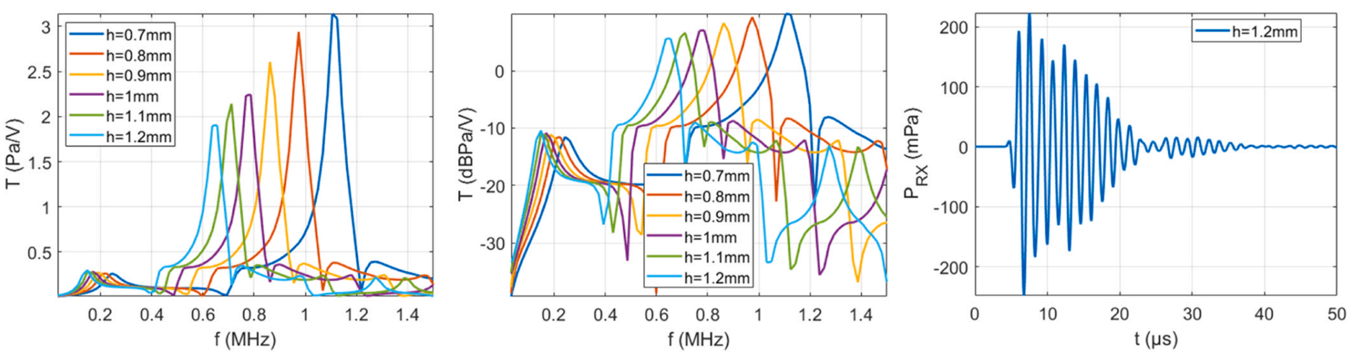

Fig. 4. Gap emission simulation when array height h is varied at fixed $t = 40$ μm $w = 10$ μm. Left: frequency domain sensitivity linear scale, center: logarithmic scale sensitivity, right: time domain response to 750 kHz, 100 % bandwidth Gabor function excitation.

The reason is that there are two emission mechanisms: cavity and edge emission (refer Fig. 1 left). These produce constructive or destructive interference, resulting in peaks or dips in AC response.

Next investigation was aimed at PVDF film thickness t effect studies. Both film thickness t and gap width w were varied to maintain same ratio for gap and edge emission. In such way, only film thickness effect was rectified, in order to confirm Eq.(2). Simulation results (thick, color curves), presented in Fig. 5, also include plane PVDF film emission (black curve, labeled "Ref") and such emission conversion into expected pressure using Eq.(2) (corresponding color, thin curves).

High transmission sensitivity, up to 4.3 Pa/V can be achieved at $t = w = 10$ μm, at 1 μm it can reach 44 Pa/V, but such value is not reasonable due to breakdown. For comparison, single PVDF film would emit 9 mPa/V, best piezocomposite-based multilayer $\lambda/4$ matched transducers reported in [24] can reach 8.9 Pa/V, yet at wider, 700 kHz at -20 dB, bandwidth. It can be noted that shape of sensitivity AC response is not changing and sensitivity is increasing as predicted by Eq. (2). Gap emission mode contains two sources: i) emission from cavity between the films and ii) emission from film edge. Fig. 6 represents new simulation results where same configuration was simulated in two setups: i) when only cavity (left) and ii) edge (center) emissions are simulated. This was achieved by removing solid-liquid interaction for edges (left, only gap emission contribution) or interaction for horizontal planes was removed (center, only edge emission contribution).

It can be noted that, for cavity emission singled, resonances do correspond to $\lambda/2$ expected frequencies. Cavity emission, if dips are ignored, is uniform over frequencies. Also, Eq.(2) can be confirmed: change of pitch $(t + w)$ from 20 μm to 40 μm is twice, pressure change is by 6 dB, changing pitch five times results in 14 dB pressure change. Smooth emission over frequencies can be expected for edge emission. Yet, at odd harmonics of $\lambda/2$ frequency emission surface does not provide push, because wave emitted from opposite tip travels up and

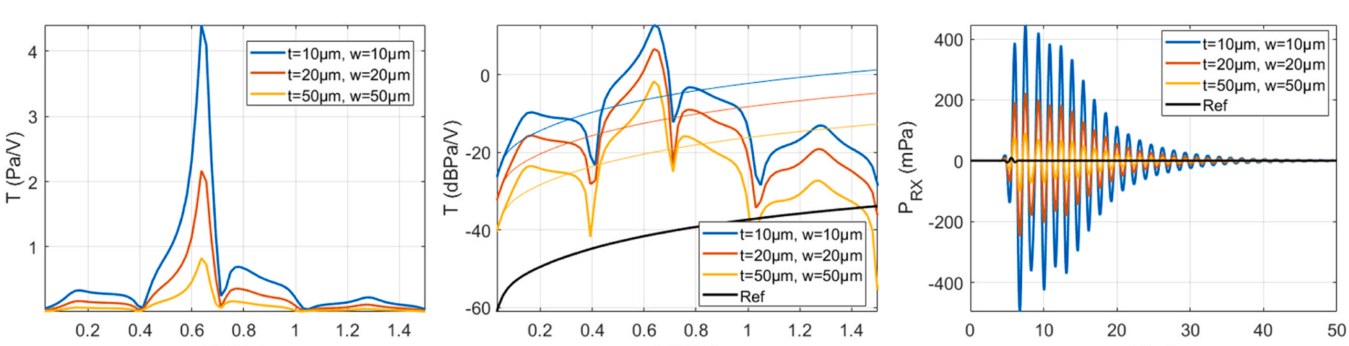

Fig. 5. Gap emission simulation when PVDF film thickness t is varied at $t = w$, $h = 1.2$ mm. Left: frequency domain sensitivity linear scale, center: logarithmic scale, right: response to 750 kHz, 100 % bandwidth Gabor function.

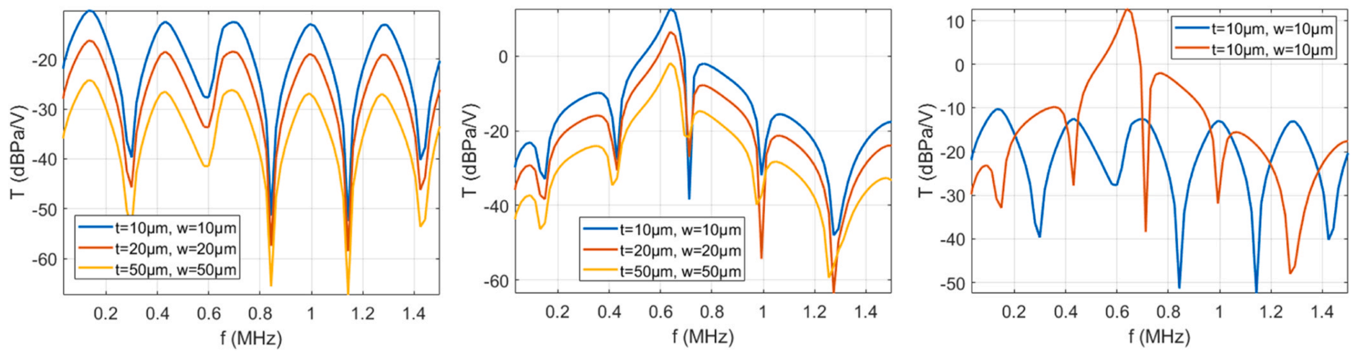

Fig. 6. Gap emission simulation at same as Fig. 5 conditions, but only cavity (left) and edge (center) emissions are considered. Right: comparison at t = 10 mm w= 10 mm, edge emission: red, cavity emission: blue.

produces destructive interference. For this reason, emission dips are at 150 kHz, 450 kHz, 750 kHz and so on. Fortunately, emission from cavity has peaks at these frequencies and therefore there is no loss of sensitivity at these frequencies. Finally, if dips are ignored, it can be noted that edge emission has a peak at 640 kHz, this is a resonance of PVDF film *h*.

Situation analyzed in Fig. 7 keeps array height *h* ratio to pitch $(t + w)$ constant. According to Eq.(2), this should correspond to same emission intensity, t/w ratio varies. In such case proportion of the pressure produced by cavity and edge varies, the larger is t/w ratio, the larger is edge emission contribution.

As can be seen from figures above, there is no significant change. The reason is that part of edge emission was expected to be reduced due to smaller emission area (smaller *t*), but smaller *t* results in larger film extension, Eq.(4). As a result, edge emission remains the same. Yet, cavity emission is affected by volume fraction (see Eq.(4): VF=$t/(t + w)$). Equivalent velocity and density (impedance) of such array for airborne wave were evaluated by registering the wave passing through and solving plate resonance inverse solution [33]. Results are presented in Fig. 7 right. Grey circles correspond to (left to right) $t = 10$ μm, 20 μm and 50 μm. Equivalent acoustic velocity of such plate remains almost constant, but density varies, therefore at low *VF* (e.g. at $t = 10$ μm *VF* is 0.17, Z_{eq} is 500 Rayl) impedance is close to air and plate resonance is not pronounced. Yet, at high VF (e.g. at $t = 50$ μm *VF* is 0.83, Z_{eq} is 2.6 kRayl) impedance is six times higher than air and plate resonance becomes more pronounced. This is the reason why emission is higher at 150 kHz, 450 kHz, 750 kHz, 1 MHz and 1.3 MHz: these are λ/2 resonance frequencies for air gap. It is worth to note that −20 dB bandwidth at $t = 50$ μm, w= 10 μm is 600 kHz, comparable to 700 kHz for best piezocomposite-based multilayer λ/4 matched transducers reported in [24].

Similar can be obtained if $(t + w)$ is not fixed but only *w* (Fig. 8 left, $t = 40$ μm) or *t* (Fig. 8, *w*=5 μm, center, *w*=50 μm, right,) is varied.

Large, up to 14 Pa/V transmission sensitivity can be achieved (at $t = 1$ μm *w*=5 μm). It also should be noted that produced field becomes nonuniform if gap size larger than 200 μm is used.

Analysis above suggests that thin PVDF film and small gap should be preferred. Yet, it should be noted that thin film will be capable of very small excitation voltages: with air breakdown 4 kV/mm, 10 μm gap will surge at 40 V, 50 μm – at 200 V and so on. It was assumed that electrodes are not offset from the film edge and air breakdown will prevail. Therefore, 40–50 μm film thickness was selected as optimal. Larger excitation voltages can be used if film edges are covered with protective coating. It can also be noted that gap reduction below 20 μm has little effect on emission spectrum (Fig. 8 left). Film thickness effect is less pronounced at 50 μm gap width, but sensitivity drops significantly (Eq. (2) effect).

Few essential findings can be concluded:

- cavity emission improvement is defined by *h* to pitch $(t + w)$ ratio;
- cavity resonance peak frequency is defined by λ/2 air column height *h*;
- edge emission improvement is defined by *h* to PVDF film thickness *t* ratio;
  - edge resonance peak frequency is defined by λ/2 PVDF film height *h*;
  - thin PVDF film and small gap are preferred, but limited to 40–50 μm by breakdown voltage (assuming up to 50 V excitation);
  - AC response contains large, up to −50 dB dips.

3.2. Membrane emission simulation analysis

Model drawing used for membrane emission simulation, is presented in Fig. 9.

Membrane and backing used built-in acrylic plastic material model

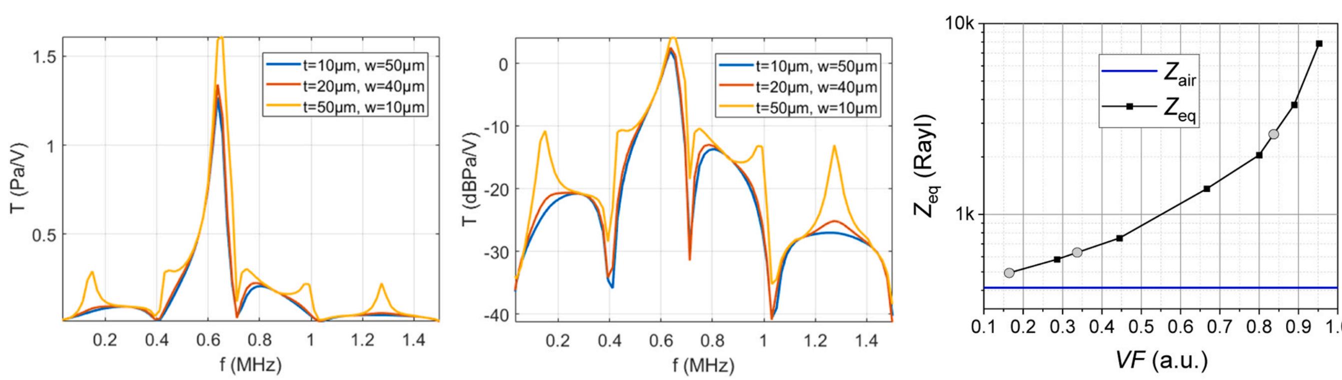

Fig. 7. Gap emission simulation when PVDF film thickness *t* is varied, but $h/(t + w)$=const= 20. Left: frequency domain sensitivity linear scale, center: logarithmic scale, right: equivalent array impedance for airborne wave.

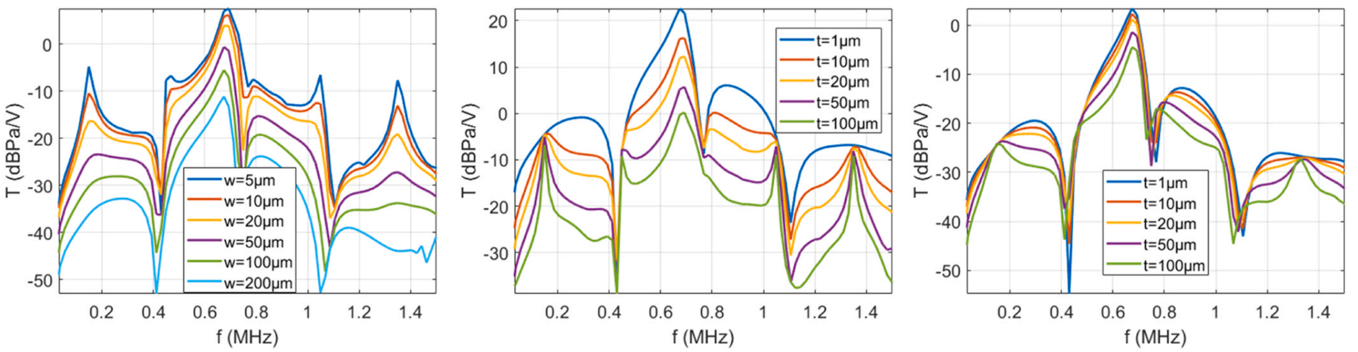

Fig. 8. Gap emission simulation when (left): gap width w is varied at fixed $t = 40$ μm; PVDF film thickness t is varied at: fixed $w = 5$ μm (center) and $w = 50$ μm (right).

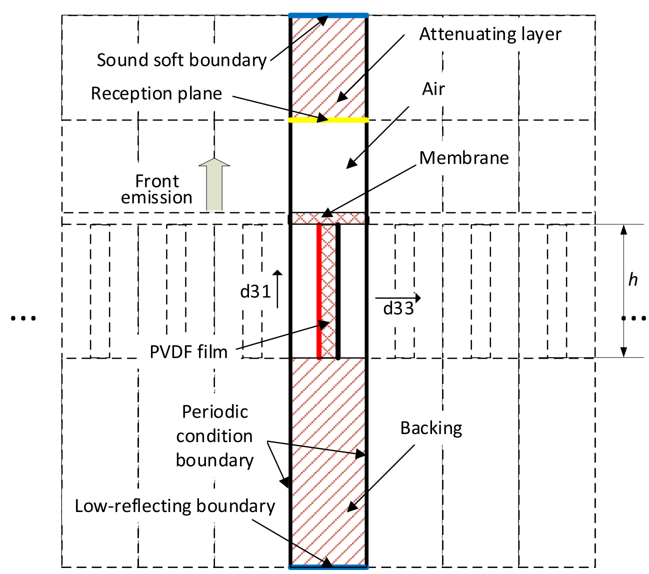

Fig. 9. FEM model geometry used for gap emission simulation.

with Young's modulus E_{ACR}= 3.1 GPa, attenuation equivalent compression wave velocity c_{ACR}= 2077.5 m/s and ρ_{ACR} = 1190 kg/m^3. Frequency-dependent attenuation used wave model with α_p= 40 dB/m and α_s= 40 dB/m at 150 kHz for longitudinal and shear waves accordingly. Low-reflecting boundary at the bottom was used to simulate an infinite backing. The rest of parameters were the same as per gap emission simulation.

Simulation results of Fig. 10 used h values corresponding to $\lambda/2$ in air at 300 kHz, 150 kHz, 100 kHz and 75 kHz. Membrane thickness h_M was 20 μm.

In this mode, equivalent film array, as solid, parameters define the AC response. It was decided to keep same array height h as in gap emission simulation, roughly 1.2 mm. Note improved response in frequency (smaller dips) and time (shorter ringdown) domain (compare to Fig. 4 or Fig. 5). In membrane emission mode behavior is different: frequency domain response is more uniform and less dependent on gap size. Amount of the produced pressure is mainly defined by film thickness t (Eq. (4) effect). See simulation results below (Fig. 11) when film thickness t is varied at fixed gap width and h 1.2 mm.

It can be noted that larger gap, differently from gap emission case, increases the emitted pressure. Effect is more pronounced for thinner PVDF film. PVDF resonance is expected at 640 kHz, same as in gap emission analysis above. Actually, resonance peak, registered in gap emission was shifted due to closely located cavity resonance, actual resonance frequency is about 680–720 kHz, can be estimated from antiresonance dip in Fig. 11. Yet, there is a slight dip at these frequencies. Dip is caused by backing and membrane: impedance of backing is close to that of PVDF so reflection is small; membrane flapping occurs at this frequency. As a results, AC response is broadband.

Gap variation effect can be evaluated from Fig. 12 below.

Explanation for emission dependence on gap size can be seen from Fig. 12 right: acoustic impedance of array is lower at larger gap, i.e. closer to air. Acoustic impedance was obtained using same technique as Fig. 7. Equivalent velocity and density (impedance) of the array suspended in air, with both ends closed by thin, 20 μm membrane, were evaluated by registering the wave passing through and solving plate resonance inverse solution [33]. Acoustic impedance of the array is 500 kRayl at w= 200 μm, close to specially designed materials. Acoustic impedance of 0.07–0.3 MRayl was reported in [38], 0.074–0.557 MRayl reported in [14], lowest, 15 kRayl value was reported in [39]. It is worth to mention that gap width is limited to $\lambda/2$ in air. If maximum operation frequency is 1.4 MHz, gap width should be w= 120 μm; at w= 200 μm

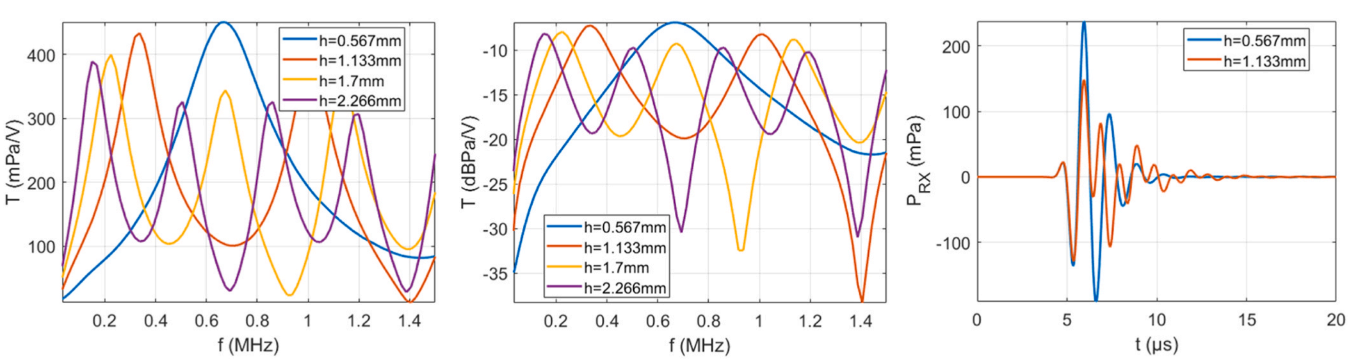

Fig. 10. Membrane emission simulation when array height h is varied at fixed $t = 40$ μm w= 100 μm. Left: frequency domain sensitivity linear scale, center: logarithmic scale sensitivity, right: temporal response to 750 kHz, 100 % bandwidth Gabor function excitation.

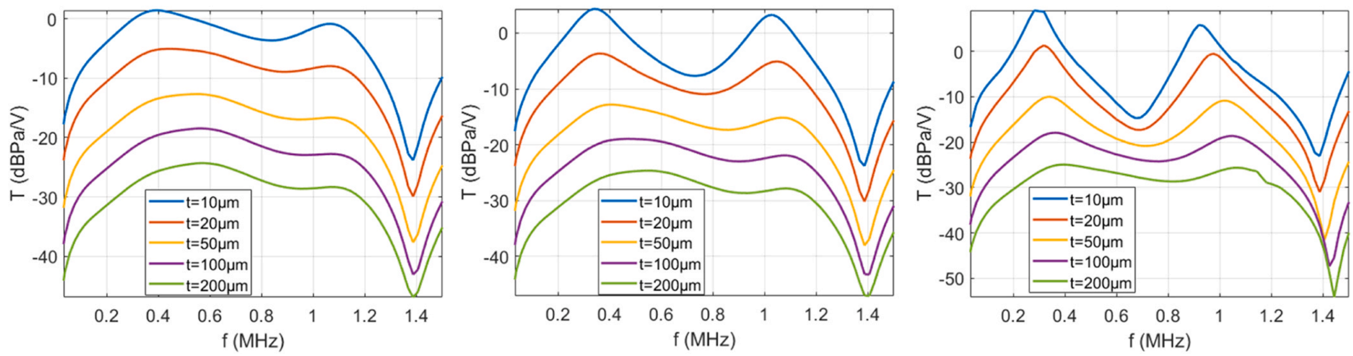

Fig. 11. Membrane emission simulation when PVDF film thickness t is varied, at fixed gap: w= 5 μm (left), w= 20 μm (center) and w= 100 μm (right).

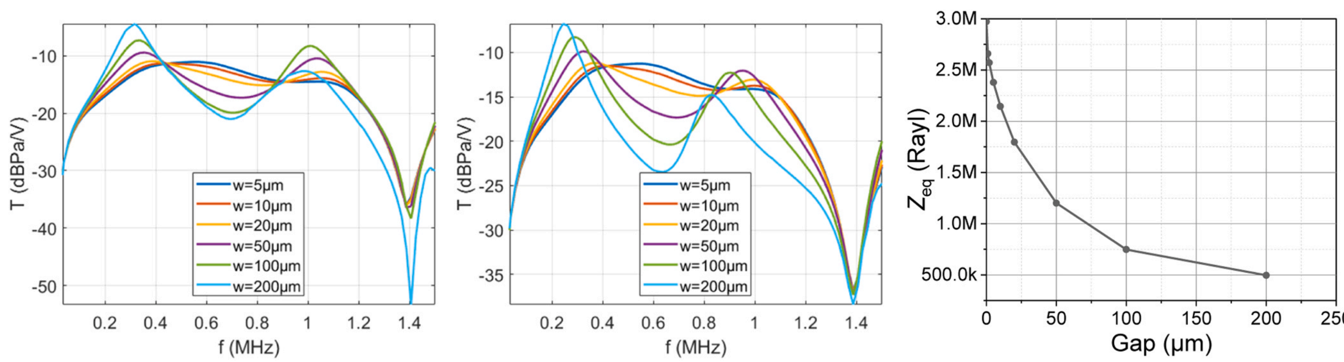

Fig. 12. Gap emission simulation when gap width is varied at fixed PVDF film thickness t = 40 μm (left: membrane thickness h_M=20 μm, center: h_M=100 μm). Right: equivalent impedance of array suspended in air.

operation is limited to 0.9 MHz. Lower impedance can be achieved with larger gap, but membrane starts to flap, reducing efficiency and implementing additional resonances. It can be assumed that thicker membrane will produce less flapping due to increased stiffness. Membrane thickness effect can be studied by comparing Fig. 12 left and center. It can be seen that thicker membrane adds more mass and flapping effect is even increased. It can be concluded, that thin, 20 μm membrane is preferred, though up to 100 μm membrane can be used if gap does not exceed 50 μm.

It is important to note that at t = 40 μm, w= 50 μm −20 dB bandwidth is 1.3 MHz, much is wider than best piezocomposite-based multilayer λ/4 matched transducers reported in [24] which achieve 700 kHz bandwidth.

Few essential findings can be concluded:

- λ/2 resonance dip of PVDF film and cavity-edge destructive interference dips have been significantly reduced due to membrane and backing effect;
- emission improvement is defined by h to PVDF film thickness t ratio;
- opposite to gap emission mode, emission is less affected by w;
- membrane up to 100 μm can be used;
- larger than 1.2 mm h can be used; yet, antiresonance peak frequency is defined by λ PVDF film height h;
- thin PVDF film is preferred, but limited to 40–50 μm by breakdown voltage;
- Essential conclusion is that membrane emission produces more uniform emission.

4. Experimental results

Experimental investigation of gapped array of PVDF films was carried out by producing an array according to parameters that were selected as optimal. The 45 nm thick PVDF film sheet with 100 nm thick sputtered aluminum electrodes (obtained from PolyK, US) was cut into 1.2 mm wide strips along d_{32} direction. Film had d_{33}= 23pC/N, d_{31}= 30pC/N. Strips were cut into 20 mm long pieces, each piece had its electrodes etched away 5 mm from each end, but at opposite sides (Fig. 13 left). Strips were placed into stack with conductive foam strips (0.3 mm thick, 390103, WE, Germany) inserted at both ends (Fig. 13 right). Electrodes in array were arranged in such way, that same polarity electrodes were facing each other.

Assembled array had a pair of fixing screws (Fig. 14 left) which were used to compress the stack. Once compressed, conductive foam formed electrically integral electrode and electrical connection to corresponding electrode face was obtained (Fig. 13 right). The gap can be regulated by changing the amount of screw torque. Minimal achievable gap on average was 55 μm, though gap size varied (see Fig. 14 right at approximately 300 μm spacing). Totally 30 PVDF strips were placed in stack, resulting in 3 mm× 10 mm emitting aperture.

Dedicated data acquisition system [36], designed and manufactured in-house was used. Assembled PVDF film array transducer was mounted (Fig. 14) on kinematic tilt positioner (5BM141, Standa, Lithuania). Excitation used bipolar excitation pulser SE-TX08–03 [34], using + /- 20 V amplitude, 50 μs duration tonebursts with frequency in range 50 kHz to 450 kHz. Reception used 20-mm-diameter air-coupled transducer (300 kHz, 650 kHz and 1 MHz center frequency used sparingly to cover all frequency range), designed and manufactured by CSIC (Spanish Research Council, Madrid, Spain) [35]. Transducers had their reception sensitivity calibrated using the technique described in [24]. Receiving transducer was mounted on 3D positioning stage (x, y, and z coordinates scanner with 10 μm resolution along x and y axes and 5 μm resolution along z axis). Pressure transmitted was measured in two configurations: i) integral received field (receiving transducer was placed at 20 mm distance from transmitting surface, assuming near-field measurements) and ii) local transmission (receiving transducer was mounted on parabolic off-axis mirror (14OAP-1–25–90-AL type from

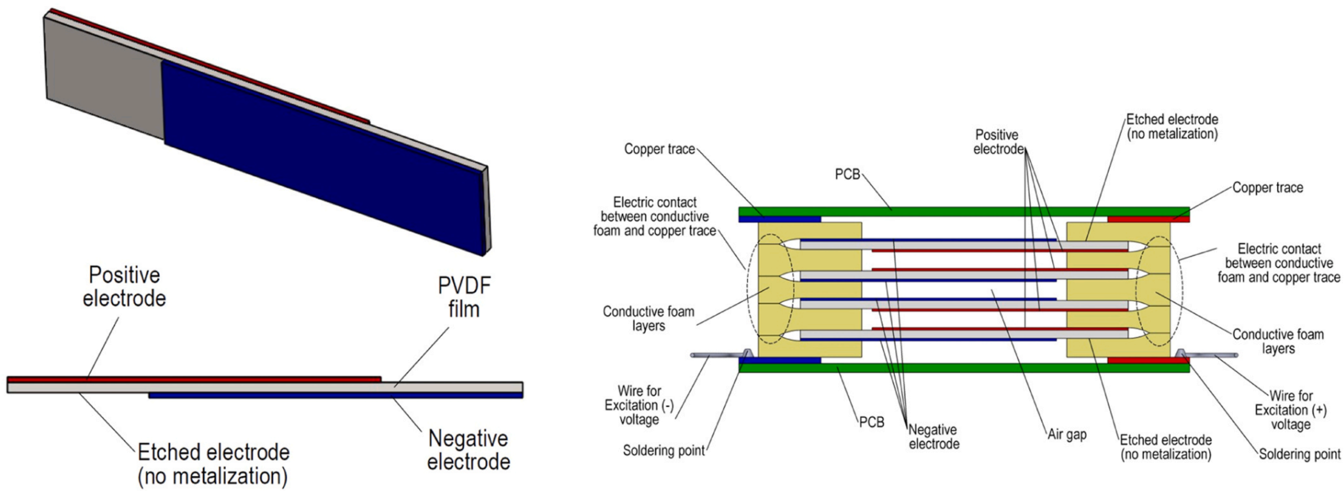

Fig. 13. Film electrodes configuration (left), array connection (right). Not to scale to keep clarity.

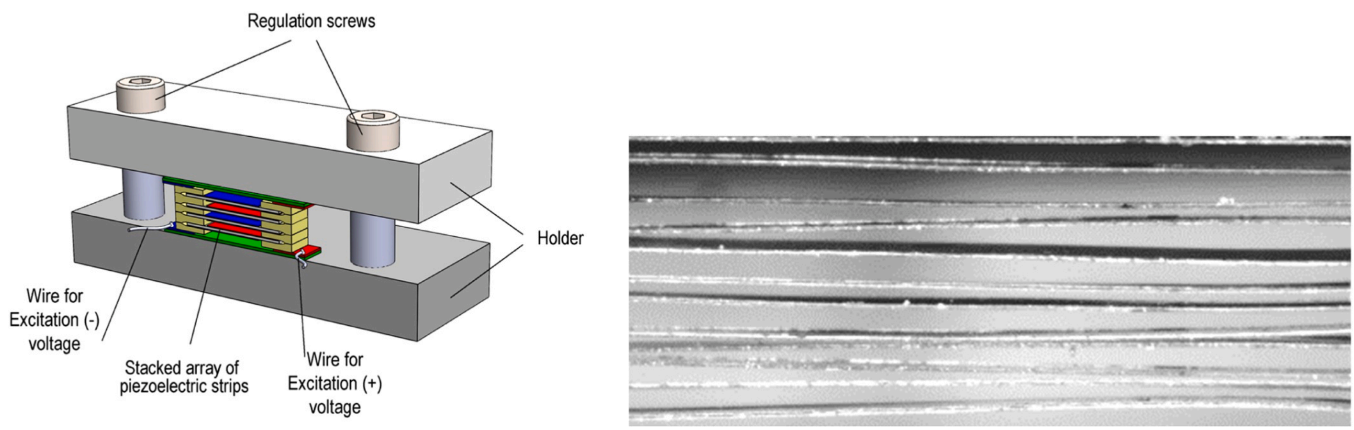

Fig. 14. Array holder with gap regulation screws and electrodes shown (left) and the actual array front view (right).

Standa Photonics, Lithuania) with focal spot, 25.4 mm, positioned on transmitting surface). Focus was scanned across emitting surface to locate highest emission point and then sensitivity AC response was measured. Received signal was amplified by low-noise preamplifier SE-RX02–00 [36] (0.1–3 MHz passband, gain programmable 7–47 dB range, 2.1 nV/$\sqrt{\text{Hz}}$ input-referred noise spectral density). Signals received were digitized using 10 bit 100 MHz ADC. Received waveform was processed using sine wave correlation (SWC) [37] in order to extract the toneburst magnitude. Extracted amplitude was corrected for the preamplifier gain, transmitting and receiving aperture difference, focal gain and attenuation in air [24]. Obtained voltage was converted to pressure in Pa using air-coupled transducer reception sensitivity, V/Pa. Excitation signal was registered using 1:100 voltage divider and second 10-bit 100 MHz ADC channel of the acquisition system. This waveform was processed using SWC [37] in order to extract the excitation toneburst magnitude. Extracted amplitude was corrected for the divider attenuation. Received pressure to transmitted voltage ratio was used as transmission sensitivity metric. Measurements were carried out with three different center frequency transducers (300 kHz, 650 kHz and 1 MHz) in order to achieve wide frequency range coverage. Measurement results were stitched together using weighted averaging. Received signal amplitude was used as a weight for stitching.

4.1. Gap emission experimental results

Experimentally measured gap transmission sensitivity AC response is presented in Figs. 15–17. Color lines are representing separate measurements with different center frequency transducer, black line is the weighted average sensitivity measurement result over 150 kHz-1.4 MHz bandwidth. Fig. 15 is for integral received field when gap width w= 200 µm, PVDF film height h= 1.2 mm and thickness t = 45 µm.

It can be noted that positions of spectral dips approximately match the simulation (Fig. 15 right). Yet, measured sensitivity is by approximately 12 dB lower at 600 kHz. This can be attributed to simulation and experimental parameters mismatch. The −20 dB bandwidth, marked by small circles on center plot, is 1.12 MHz, or 138 % of peak frequency. Note that bandwidth was measured by ignoring dips (e.g. at 400 kHz) and only extreme points were used in bandwidth evaluation.

Fig. 16 is for integral received field when gap width w= 55 µm, PVDF film height h= 3 mm and thickness t = 45 µm. The film height h was increased to 3 mm due to more convenient handling (it is quite complicated to manually cut 1.2 mm strips; also stack form is easier to maintain). Also, higher value of h produces more pressure gain.

Wider strip (h=3 mm instead of 1.2 mm in previous figure) is producing slightly higher emission (155 mPa/V instead of 58mPa/V), but bandwidth is narrower (940 kHz instead of 1.12 MHz). Spectral ripples for experimental results are smaller than those obtained in simulation. Ripples are produced by constructive and destructive interference of gap and edge emissions. Simulation used uniform emission surface, but real-world realization has small manufacturing variations therefore interference is not so strongly pronounced. Fig. 17 is for local peak emission (receiving transducer beam is focused on transmitting surface where

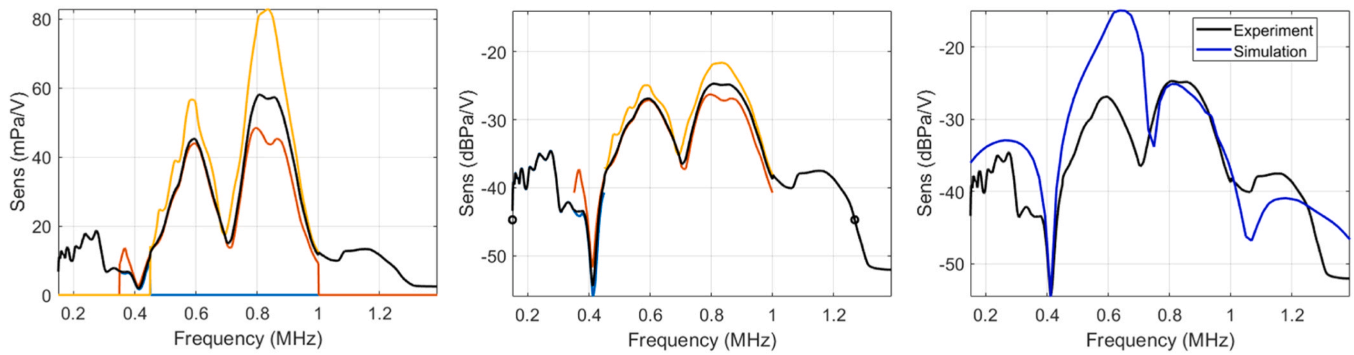

Fig. 15. Experimentally measured integral gap emission sensitivity in linear (left) and logarithmic (center) scale, comparison to simulation (right). Gap width w= 200 µm, PVDF film height h= 1.2 mm thickness t = 45 µm.

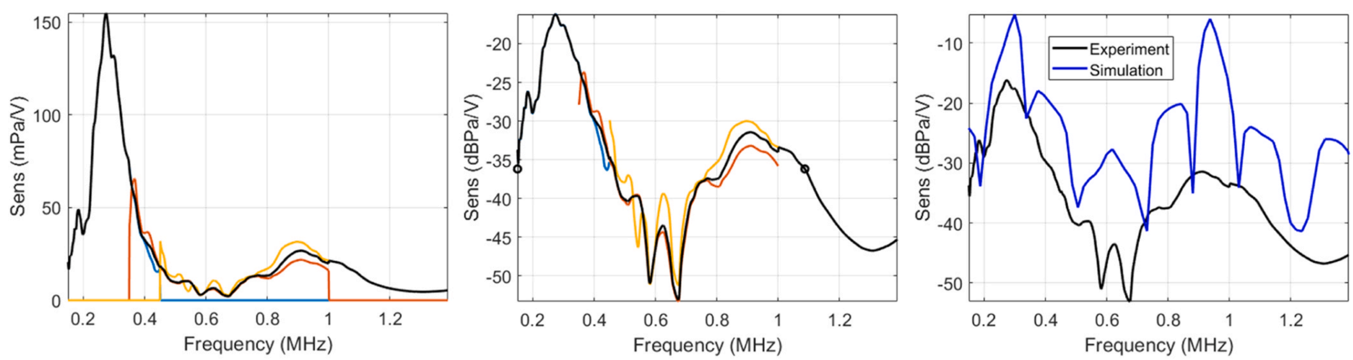

Fig. 16. Experimentally measured integral gap emission sensitivity in linear (left) and logarithmic (center) scale, comparison to simulation (right). Height h= 3 mm, gap width w= 55 µm, PVDF film thickness t = 45 µm.

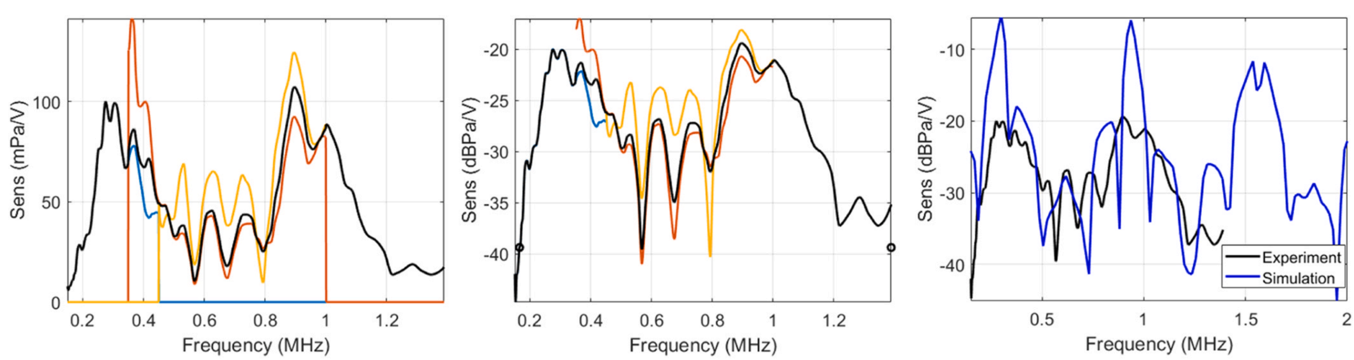

Fig. 17. Experimentally measured local peak gap emission sensitivity in linear (left) and logarithmic (center) scale comparison to simulation (right). Height h= 3 mm, gap width w= 55 µm, PVDF film thickness t = 45 µm.

transduction is maximal) for same as Fig. 16 array parameters.

In this case transduction sensitivity AC response is more uniform therefore bandwidth is broader than the measurement range, it can only be extrapolated from simulation (note that for this figure right frequency range is broader that used before). Though absolute sensitivity is similar to integral measurements (Fig. 16).

4.2. Membrane emission experimental results

Membrane emission (refer Fig. 1 right) was realized by attaching the waterslide decal paper on emitting surface. Membrane thickness was not measured, manufacturer has specified 23 µm thickness. Backing was implemented by using thick, gel-type UV curable polymer which was smeared over the opposite surface to form backing. Approximately 2 mm backing was used. Array height h was 3 mm. Intermediate results, when only membrane on front emitting surface was attached, but backing was not applied, are presented in Fig. 18 and Fig. 19.

Transmission sensitivity is twice higher than before membrane application, peaks and dips are less pronounced than in simulation. Extremely broad bandwidth can be expected for local peak sensitivity, yet integral transduction sensitivity has moderate bandwidth, same as in case without membrane (940 kHz).

Final results, when by UV-curable polymer backing was applied, are presented in Figs. 20 and 21.

It is worth to mention that in real-world situation, surface of membrane and backing are nonuniform. Also, height of the PVDF film h can not be maintained for every individual strip because of manual cutting. Then, some oblique force on PVDF film edge is developed. In such case Lamb/plate waves, essentially A0, are excited in the PVDF film (Fig. 22). Two disturbing effects were simulated: i) variable (variation 250 µm)

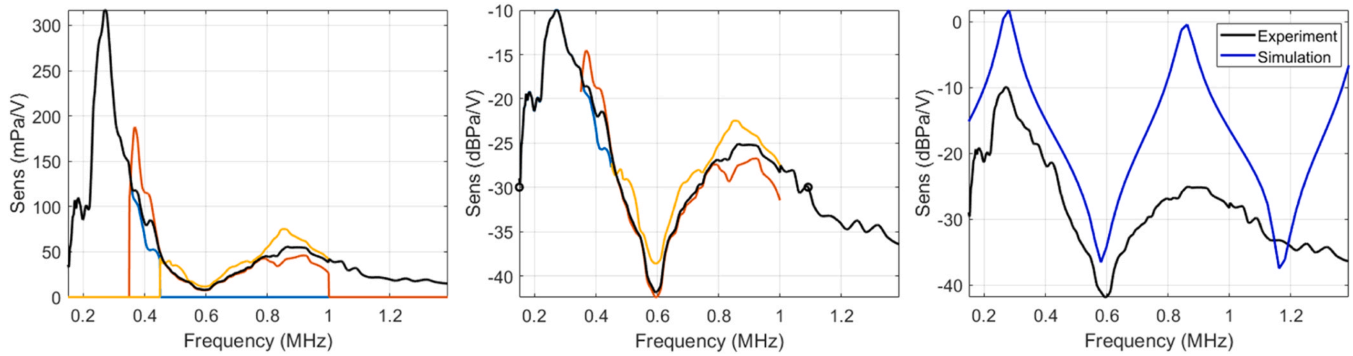

Fig. 18. Experimentally measured integral emission sensitivity: membrane on top but bottom free. In linear (left), logarithmic (center) scale and comparison to simulation (right). *h*= 3 mm, *w*= 55 μm, *t* = 45 μm, *d*= 23 μm.

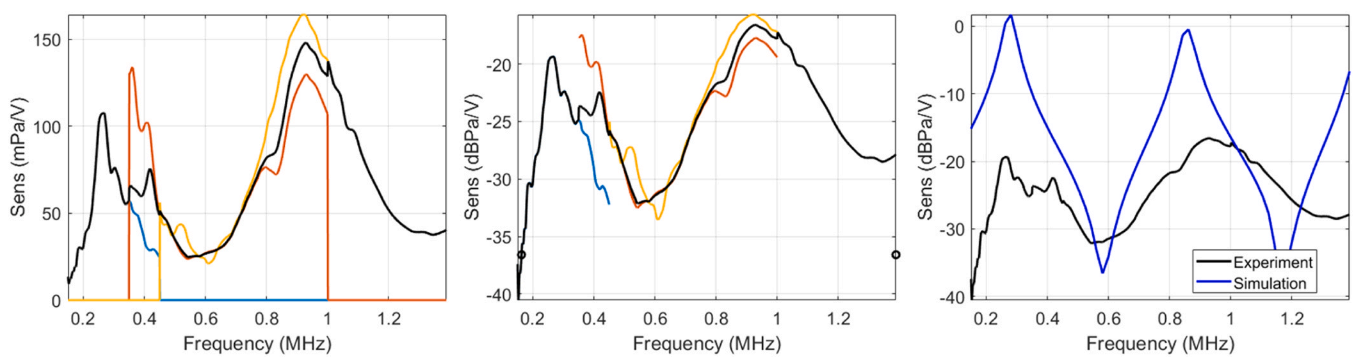

Fig. 19. Experimentally measured local peak emission sensitivity: membrane on top but bottom free. In linear (left), logarithmic (center) scale and comparison to simulation (right). *h*= 3 mm, *w*= 55 μm, *t* = 45 μm, *d*= 23 μm.

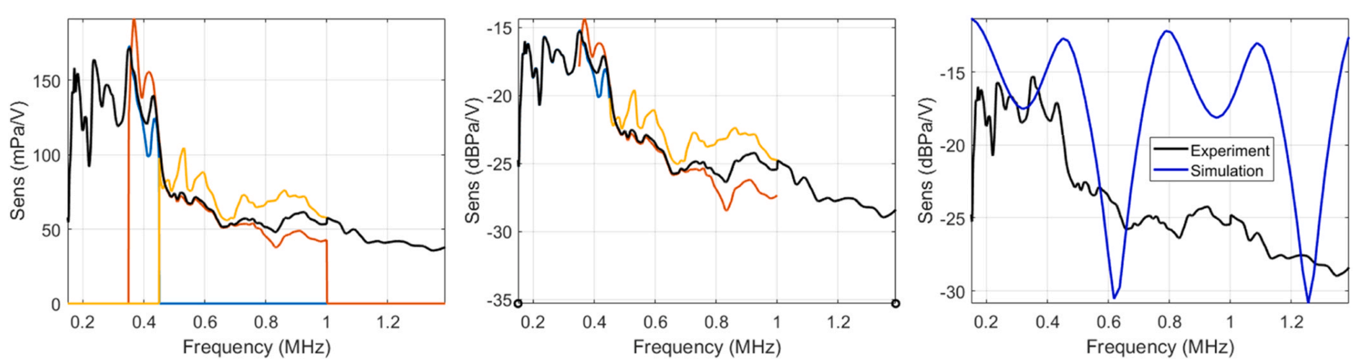

Fig. 20. Experimentally measured integral sensitivity: membrane on top, bottom backed. In linear (left), logarithmic (center) scale and comparison to simulation (right). *h*= 3 mm, *w*= 55 μm, *t* = 45 μm, *d*= 23 μm.

height h (Fig. 22a) array and ii) same *h* array, but inclined backing (Fig. 22c) in order to induce bending. Variable height is also inducing PVDF film buckling which also causes membrane surface distortions (Fig. 22b). Array of same h was backed against inclined backing, film edge was also inclined correspondingly. This induced uniform bending of array. Produced pressure for variable *h* array (red curve Fig. 22d) and uniformly bending array (yellow curve Fig. 22d) was compared against uniform array with no bending and no h variation (blue curve Fig. 22d).

It can be noted that influence of bending motion on transduction performance is minimal (see Fig. 22d), it can be concluded that vertical force is mainly defined by d31 piston-like mode.

Results are summarized in Figs. 23 and 24. Fig. 23 is representing lower and upper passband frequencies along with achieved bandwidth for −6 dB (Fig. 23 left) and −20 dB (Fig. 23 right) cutoff. Best-performing λ/4-matched transducers [35], used as calibrated standard in this research are also included for comparison.

It can be noted that conventional, λ/4-matched transducers, have bandwidth proportional to their center frequency. It is accustomed to express the bandwidth as fraction of center frequency. Fractional bandwidth (left) and peak transmission sensitivity (right) are presented in Fig. 24.

It can be concluded that transduction bandwidth achieved is significantly broader: λ/4-matched transducers have approximately 100 % bandwidth, which is impressive for air-coupled transducers, but new type transducer can reach beyond 250 % bandwidth. This comes at the expense of reduced transduction: while λ/4-matched transducers can reach up to 21.4 dBPa/V (11.7 Pa/V), new type can only provide −10 dBPa/V (0.32 Pa/V). Also, from Figs. 15–21, it can be noted that transduction AC response for new type transducer is nonuniform. Yet, spectral losses can be compensated up to 20 dB, using programmable

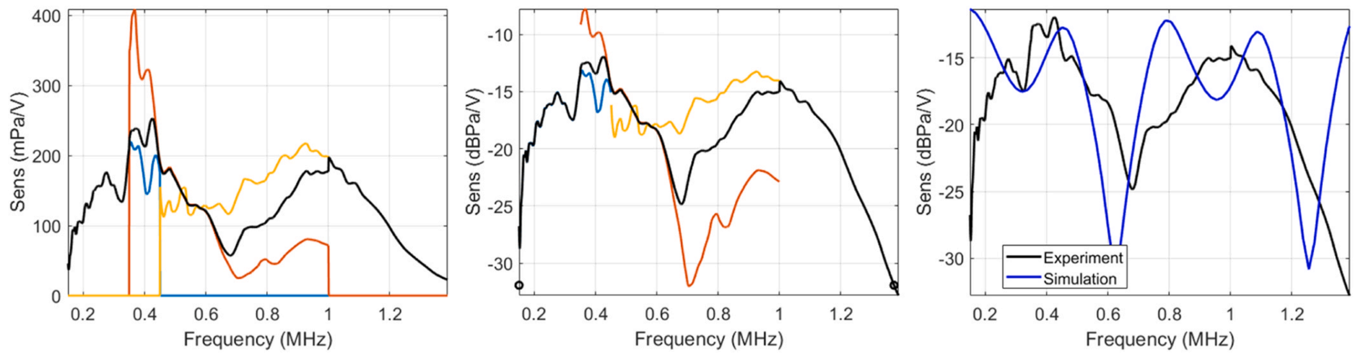

Fig. 21. Experimentally measured local peak sensitivity: membrane on top, bottom backed. In linear (left), logarithmic (center) scale and comparison to simulation (right). h= 3 mm, w= 55 µm, t = 45 µm, d= 23 µm.

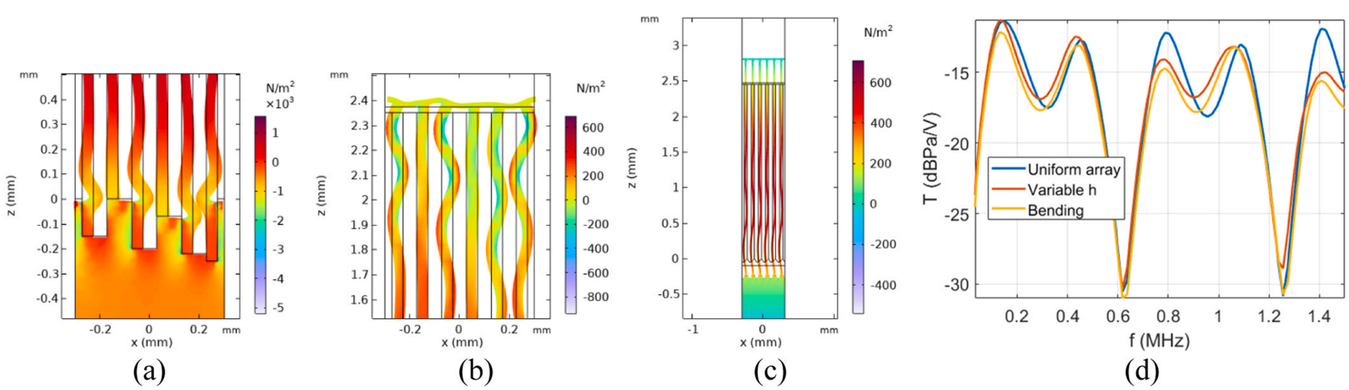

Fig. 22. Simulation result for Fig. 21 configuration with more disturbing effects: nonuniform PVDF film height h (a,b); inclined backing surface to induce film bending (c) and AC response comparison. h= 3–3.25 mm, w= 55 µm, t = 45 µm, d= 23 µm, deformation gain in 10^6 for a-c.

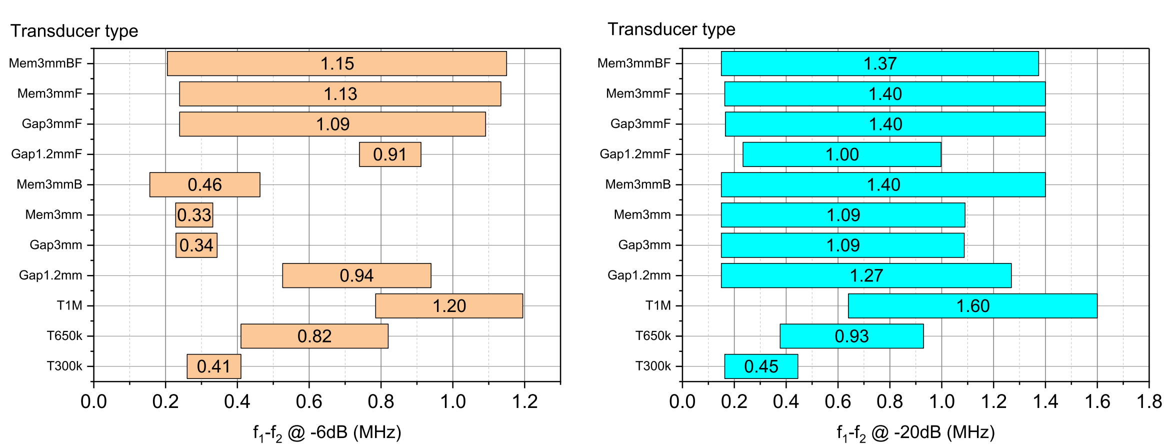

Fig. 23. Comparison of lower, upper frequency and bandwidth at −6 dB (left) and −20 dB (right) for transducer types used in this study. Legend: "T300k", "T650k" and "T1M" are for λ/4-matched transducers [35] with corresponding center frequency; "Gap1.2 mm", "Gap3mm", "Gap1.2mmF" and "Gap3mmF" are for gap transmission with corresponding stack height; "Mem3mm", "Mem3mm", "Mem3mmB" and "Mem3mmBF" are for membrane emission; letter "F" is to distinguish local (focused) emission from integral measurements; letter "B" indicates that backing was applied.

spectrum spread spectrum signals [40,41]. In such case, uniformity of AC response is not essential, it is more important to achieve wide spectral coverage within 20 dB range. This is the reason why bandwidth was measured at −20 dB cutoff.

5. Conclusions

Broader use of the air-coupled ultrasound is limited by the significant acoustic impedance mismatch between media and transducer material. The novelty of the approach proposed here is in special arrangement of piezoelement. It is proposed to change the orientation of the piezoelement and arrangement, by using an array of PVDF films placed parallel to each other with air gaps between. Films are oriented in such way that length extension is aligned with emission direction. Two distinct operation modes were considered: i) emission from the gaps ii) emission from membrane attached to the edges at array top with lower edges backed.

In gap emission mode, the transduction efficiency is increased because of two mechanisms. The pressure produced by the expansion of the individual films is concentrated into narrow gap. Also, emission of

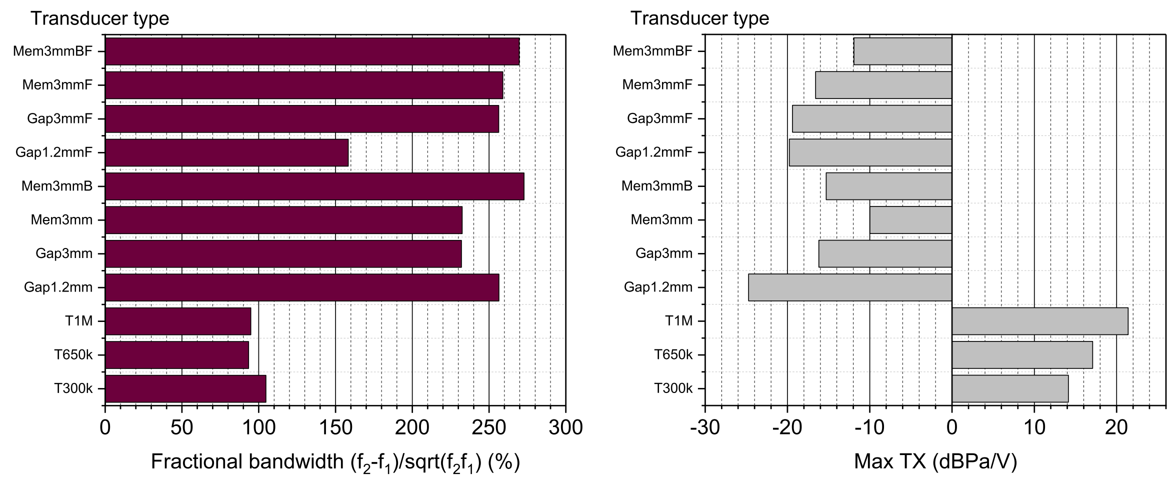

Fig. 24. Comparison of fractional bandwidth at −20 dB (left) and transmission sensitivity (right) for transducer types used in this study. Same legend as Fig. 23.

edges is large due to length extension. Length extension is much higher than expansion if film height is larger than film thickness. Equivalent acoustic impedance of such array is very low at low volume fraction (e.g. at film thickness 10 μm and gap with 50 μm acoustic impedance is 500 Rayl, very close to air, 413 Rayl). Simulation indicates that high transmission sensitivity, up to 4.3 Pa/V or even 44 Pa/V (t = 1 μm, if low excitation voltage is acceptable) can be achieved. However, very thin films and small gaps can not be achieved experimentally. Therefore, experimentally evaluated transmission sensitivity was lower, 155 mPa/V. For comparison, single PVDF film, emitting in a usual way, can only reach 9 mPa/V. Impressive, 256 % fractional bandwidth was confirmed experimentally. However, presence of two emission sources with different delays creates destructive interference at frequencies where phase is opposite.

In membrane emission mode, only length extension is used, pressure emitted is increased due to large membrane displacement and better match to air. Matching to air is at lower extent: array acoustic impedance is 500 kRayl at PVDF film thickness 40 μm and 200 μm air gap. Smaller impedance can be achieved with wider gap, but membrane starts to flap at frequencies which exceed λ/2 in air. If maximum operation frequency is lower than 1.4 MHz, gap width can be increased to obtain lower impedance. Membrane displacement is maximized if PVDF films with large transverse piezoelectric coefficient d_{31} (e.g. uniaxially stretched) are used. Experimentally evaluated transmission sensitivity for membrane emission mode was 320 mPa/V. Much wider than conventional transducers, 270 % fractional bandwidth was confirmed experimentally for membrane emission mode.

CRediT authorship contribution statement

Valdas Eidukynas: Writing – original draft, Visualization, Validation, Software, Resources, Data curation. **Luca De Marchi:** Writing – review & editing, Writing – original draft, Validation, Methodology, Formal analysis. **Andrius Chaziachmetovas:** Writing – review & editing, Writing – original draft, Validation, Resources, Investigation, Formal analysis, Data curation. **Linas Svilainis:** Writing – review & editing, Writing – original draft, Supervision, Software, Project administration, Methodology, Funding acquisition, Conceptualization.

Declaration of Competing Interest

Linas Svilainis reports financial support was provided by Research Council of Lithuania. Linas Svilainis has patent AIR-COUPLED ULTRASOUND TRANSDUCER WITH ARRAY OF VERTICALLY PARALLEL PIEZOELECTRIC ELEMENTS pending to Kaunas University of Technology. If there are other authors, they declare that they have no known competing financial interests or personal relationships that could have appeared to influence the work reported in this paper.

Acknowledgements

This work was funded by a Grant No. S-MIP-23–133 from the Research Council of Lithuania (LMTLT).

Data availability

Data will be made available on request.

References

[1] A.S. Dzunuzovic, et al., Electrical properties of x(0.75 Na1/2Bi1/2TiO3-0.25SrTiO3)(1-x)PVDF flexible piezoceramic polymer composites, Sens. Actuators A Phys. 392 (2025) 116704, https://doi.org/10.1016/j.sna.2025.116704.
[2] P. Chen, et al., Improving wideband performance for ScAlN based piezoelectric MEMS speaker by multi-mode excitation, Sens. Actuators A Phys. 393 (2025) 116812, https://doi.org/10.1016/j.sna.2025.116812.
[3] K.S. Ramadan, D. Sameoto, S. Evoy, A review of piezoelectric polymers as functional materials for electromechanical transducers, Smart Mater. Struct. 23 (3) (2014) 033001, https://doi.org/10.1088/0964-1726/23/3/033001.
[4] I. Solodov, et al., New opportunities for NDE with air-coupled ultrasound, NDT E Int 39 (3) (2006) 176–183, https://doi.org/10.1016/j.ndteint.2005.07.002.
[5] S.J. Sanabria, et al., Air-coupled ultrasound as an accurate and reproducible method for bonding assessment of glued timber, Wood Sci. Technol. 45 (4) (2011) 645–659, https://doi.org/10.1007/s00226-010-0357-z.
[6] T.Y. Sun, et al., A novel internal crack detection method for photovoltaic (PV) panels based on the air-coupled ultrasonic, Sens. Actuators A Phys. 392 (2025) 116642, https://doi.org/10.1016/j.sna.2025.116642.
[7] D.W. Schindel, D.A. Hutchins, Through-thickness characterization of solids by wide-band air-coupled ultrasound, Ultrasonics 33 (1) (1995) 11–17, https://doi.org/10.1016/0041-624X(95)00011-Q.
[8] J.Y. Tang, et al., Design, fabrication and characterization of Emfi-based ferroelectretair-coupled ultrasonic transducer, Sens. Actuators A Phys. 296 (2019) 52–60, https://doi.org/10.1016/j.sna.2019.06.044.
[9] F. Lionetto, A. Tarzia, A. Maffezzoli, Air-coupled ultrasound: a novel technique for monitoring the curing of thermosetting matrices, IEEE Trans. Ultrason. Ferroelectr. Freq. Control 54 (7) (2007) 1437–1444, https://doi.org/10.1109/TUFFC.2007.404.
[10] T. Pernu, J. Saarilahti, T. Sillanpää, Real-time frequency matching circuit for a high sensitivity cMUT-based gas flow sensor, Sens. Actuators A Phys. 383 (2025) 116252, https://doi.org/10.1016/j.sna.2025.116252.
[11] S. Meyer, et al., Non-contact evaluation of milk-based products using air-coupled ultrasound, Meas. Sci. Technol. 17 (7) (2006) 1838–1846, https://doi.org/10.1088/0957-0233/17/7/023.
[12] T.E.G. Alvarez-Arenas, D. Sancho-Knapik, J.J. Peguero-Pina, E. Gil-Pelegrín, Noncontact and noninvasive study of plant leaves using air-coupled ultrasounds, Appl. Phys. Lett. 95 (19) (2009) 193702, https://doi.org/10.1063/1.3263138.
[13] V.T. Rathod, A review of acoustic impedance matching techniques for piezoelectric sensors and transducers, Sensors 20 (14) (2020) 4051, https://doi.org/10.3390/s20144051.
[14] T.E.G. Alvarez-Arenas, Acoustic impedance matching of piezoelectric transducers to the air, IEEE Trans. Ultrason. Ferroelectr. Freq. Control 51 (5) (2004) 624–633, https://doi.org/10.1109/TUFFC.2004.1320834.

[15] J.J. Gu, et al., Lowering the sound transmission loss of impedance-matching structures: Data-driven optimization assisted with a priori knowledge, Mater. Des. 232 (2023) 112091, https://doi.org/10.1016/j.matdes.2023.112091.

[16] T. Gudra, K.J. Opielinski, Influence of acoustic impedance of multilayer acoustic systems on the transfer function of ultrasonic airborne transducers, Ultrasonics 40 (1-8) (2002) 457–463, https://doi.org/10.1016/S0041-624X(02)00159-2.

[17] T.E.G. Alvarez-Arenas, L. Diez, Novel impedance matching materials and strategies for Air-Coupled piezoelectric transducers, IEEE Sens. (2013) 191494–191497.

[18] L. Amoroso, et al., Novel nanocomposite materials for improving passive layers in Air-coupled ultrasonic transducer applications, IEEE Int. Ultrason. Symp (IUS) (2019) 2608–2611, https://doi.org/10.1109/ultsym.2019.8925712.

[19] C. Ferraro, et al., Light and strong SiC networks, Adv. Funct. Mater. 26 (10) (2016) 1636–1645, https://doi.org/10.1002/adfm.201504051.

[20] H. Tanaka, S. Machida, M. Nanri, Active acoustic impedance matching using CMUT structure, in: proceedings of, IEEE Int. Ultrason. Symp (IUS) (2021), https://doi.org/10.1109/IUS52206.2021.9593796.

[21] H. Tanaka, S. Machida, M. Nanri, Fabrication and evaluation of MUT-Type acoustic metamaterial for impedance matching, IEEJ Trans. Electr. Electron. Eng. 19 (4) (2024) 586–594, https://doi.org/10.1002/tee.24038.

[22] A. Ba, et al., Soft porous silicone rubbers with ultra-low sound speeds in acoustic metamaterials, Sci. Rep. 7 (2017) 40106, https://doi.org/10.1038/srep40106.

[23] Z. Li, et al., Broadband gradient impedance matching using an acoustic metamaterial for ultrasonic transducers, Sci. Rep. 7 (2017) 42863, https://doi.org/10.1038/srep42863.

[24] L. Svilainis, A. Chaziachmetovas, P. Kaskonas, T.E.G. Alvarez-Arenas, Ultrasonic needle hydrophone calibration in air by a parabolic off-axis mirror focused beam using three-transducer reciprocity, Ultrasonics 133 (2023) 107025, https://doi.org/10.1016/j.ultras.2023.107025.

[25] M. Toda, J. Dahl, PVDF corrugated transducer for ultrasonic ranging sensor, Sens. Actuators A Phys. 134 (2) (2007) 427–435, https://doi.org/10.1016/j.sna.2006.07.018.

[26] L. Svilainis, et al., Miniature ferroelectret microphone design and performance evaluation using laser excitation, IEEE Trans. Ultrason. Ferroelectr. Freq. Control 69 (12) (2022) 3392–3401, https://doi.org/10.1109/TUFFC.2022.3220082.

[27] D.A. Hutchins, T.J. Robertson, D.R. Billson, New designs of focused air-coupled ultrasonic transducer, Rev. De. Acust. 33 (2002) 3–4.

[28] T.E.G. Alvarez-Arenas, J. Camacho, C. Fritsch, Passive focusing techniques for piezo electric air-coupled ultrasonic transducers, Ultrasonics 67 (2016) 85–93, https://doi.org/10.1016/j.ultras.2016.01.001.

[29] J.J. Wang, Z.F. Shi, Z.J. Han, Analytical solution of piezoelectric composite stack transducers, J. Intell. Mater. 24 (13) (2013) 1626–1636, https://doi.org/10.1177/1045389X13479185.

[30] S. Takahashi, H. Ohigashi, Ultrasonic imaging using air-coupled P(VDF/TrFE) transducers at 2 MHz, Ultrasonics 49 (4-5) (2009) 495–498, https://doi.org/10.1016/j.ultras.2008.10.020.

[31] S. Mohammadpourfazeli, et al., Future prospects and recent developments of polyvinylidene fluoride (PVDF) piezoelectric polymer; fabrication methods, structure, and electro-mechanical properties, RSC Adv. 13 (1) (2022) 370–387, https://doi.org/10.1039/d2ra06774a.

[32] H. Tanaka, S. Machida, Super broadband acoustic impedance matching by MUT-type acoustic metamaterial, Electron. Commun. Jpn. 103 (1-4) (2020) 38–47, https://doi.org/10.1002/ecj.12228.

[33] Z. Nakutis, P. Kaskonas, D. Liaukonis, L. Svilainis, Air-Coupled ultrasound spectroscopy air parameters compensation technique, IEEE Sens. J. 24 (8) (2024) 12667–12675, https://doi.org/10.1109/JSEN.2024.3369508.

[34] L. Svilainis, V. Dumbrava, A. Chaziachmetovas, A. Aleksandrovas, Pulser for arbitrary width and position square pulse trains generation, in: proceedings of, IEEE Int. Ultrason. Symp (IUS) (2012), https://doi.org/10.1109/ULTSYM.2012.0438.

[35] T.E.G. Alvarez-Arenas, Air-Coupled piezoelectric transducers with active polypropylene foam matching layers, Sensors 13 (5) (2013) 5996–6013, https://doi.org/10.3390/s130505996.

[36] L. Svilainis, et al., Electronics for ultrasonic imaging system, Electron. Elektro 20 (7) (2014) 51–56, https://doi.org/10.5755/j01.eee.20.7.8024.

[37] V. Dumbrava, L. Svilainis, The automated complex impedance measurement system, Electron. Elektro 4 (76) (2007) 59–62.

[38] T.E.G. Alvarez-Arenas, A nondestructive integrity test for membrane filters based on air-coupled ultrasonic spectroscopy, IEEE Trans. Ultrason. Ferroelectr. Freq. Control 50 (6) (2003) 676–685, https://doi.org/10.1109/TUFFC.2003.1209555.

[39] T.E. Gómez, F.M. de Espinosa, Fabrication and characterization of silica aerogel films for air-coupled piezoelectric transducers in the megahertz range, in: Proceedings of IEEE International Ultrasonics Symposium (IUS) 2002 1107-1110 (2002), doi: 10.1109/ULTSYM.2002.1192487.

[40] L. Svilainis, A. Rodriguez-Martinez, A. Chaziachmetovas, A. Aleksandrovas, Ultrasound transmission spectral compensation using arbitrary position and width pulse sets, IEEE Trans. Instrum. Meas. 67 (8) (2018) 1778–1785, https://doi.org/10.1109/TIM.2018.2809838.

[41] M. Tayyib, L. Svilainis, SNR equalization in non-contact resonant ultrasound spectroscopy measurements, NDT E Int. 154 (2025) 103386, https://doi.org/10.1016/j.ndteint.2025.103386.

[42] R. Carter, R. Kensley, Introduction to Piezoelectric Transducers, Piezo.com, 2022. ⟨https://piezo.com/pages/piezoelectric-transducers-abstract⟩.

Linas Svilainis received PhD degree from Kaunas University of Technology (Lithuania) in 1996. Since 2009 he is a Full time Professor at the Department of Electronics Engineering, Kaunas University of Technology, Lithuania. His current areas of research are design and optimization of ultrasound electronics; ultrasonic signal processing; time delay (time-of-flight, ToF) estimation; spread spectrum signals; air-coupled ultrasound; large scale LED video displays; electromagnetic compatibility and EMI protection of electronic systems.

Valdas Eidukynas received PhD degree from the Kaunas University of Technology (Lithuania) in 1996. Since 2019 he is a Full time Professor at the Department of Mechanical Engineering, Kaunas University of Technology, Lithuania. His current research interests are Computer-aided modeling and numerical analysis methods and tools in static and dynamic analysis of solid bodies and fluid-structure interaction under the static, dynamic, seismic, and thermal loading as acoustic and elastic waves propagation in various materials as well multiphysics analysis including piezo effects.

Luca De Marchi received the M.Sc. and Ph.D. degrees in electronics engineering from the University of Bologna, Bologna, Italy, in 2002 and 2006, respectively. He is currently an Associate Professor of Electronics with the University of Bologna. His research interests include multiresolution and adaptive signal processing, with a particular emphasis on SHM applications.

Andrius Chaziachmetovas received PhD degree from the Kaunas University of Technology (Lithuania) in 2007. Since 2009, he is an Associate Professor with the Department of Electronics Engineering, Kaunas University of Technology, Kaunas. His current research interests include ultrasonic measurements, ultrasound electronics, high-voltage pulsers, software development, embedded systems, and time of flight estimation.